Molecular Crystals and Liquid Crystals
Publication details, including instructions for authors and subscription information:
http://www.tandfonline.com/loi/gmcl20

Surface Alignment, Anchoring Transitions, Optical Properties and Topological Defects in Nematic Bent-Core Materials C7 and C12

B. Senyuk [a], Y.-K. Kim [a], L. Tortora [a], S.-T. Shin [b], S. V. Shiyanovskii [a] & O. D. Lavrentovich [a]

[a] Liquid Crystal Institute and Chemical Physics Interdisciplinary Program, Kent State University, Kent, OH, USA

[b] Liquid Crystal Display Research and Development Center, Samsung Electronics Corporation, Korea

Version of record first published: 14 Jun 2011

To cite this article: B. Senyuk, Y.-K. Kim, L. Tortora, S.-T. Shin, S. V. Shiyanovskii & O. D. Lavrentovich (2011): Surface Alignment, Anchoring Transitions, Optical Properties and Topological Defects in Nematic Bent-Core Materials C7 and C12, Molecular Crystals and Liquid Crystals, 540:1, 20-41

To link to this article: http://dx.doi.org/10.1080/15421406.2011.568324

Mol. Cryst. Liq. Cryst., Vol. 540: pp. 20–41, 2011

ISSN: 1542-1406 print/1563-5287 online
DOI: 10.1080/15421406.2011.568324

Surface Alignment, Anchoring Transitions, Optical Properties and Topological Defects in Nematic Bent-Core Materials C7 and C12

B. SENYUK,[1] Y.-K. KIM,[1] L. TORTORA,[1] S.-T. SHIN,[2] S. V. SHIYANOVSKII,[1] AND O. D. LAVRENTOVICH[1]

[1]Liquid Crystal Institute and Chemical Physics Interdisciplinary Program, Kent State University, Kent, OH, USA
[2]Liquid Crystal Display Research and Development Center, Samsung Electronics Corporation, Korea

We address the status of oxadiazole mesogens, C7 and C12, reported to show the biaxial nematic phase, by exploring material aspects (chemical stability, surface anchoring, optical and dielectric properties, topological defects) linked to the type of nematic order. We demonstrate that the isogyres splitting in conoscopic patterns of homeotropic state depends on sample thickness and is associated with variations of molecular tilt along the normal to substrates. We observe isolated topological point defects (boojums and hedgehogs), as well as nonsingular "escaped" disclinations pertinent only to the uniaxial nematic order. Our conclusion is that C7 and C12 feature only a uniaxial nematic phase and the apparent biaxiality is caused by surface effects.

Keywords Anchoring transition; bent-core nematics; biaxial phase; conoscopy; topological defects

1. Introduction

Many of current liquid crystal (LC) electro-optics and display applications use thermotropic uniaxial nematics (N_u) showing anisotropy of physical properties with two principal directions, along and perpendicular to the director $\hat{\mathbf{n}} \equiv -\hat{\mathbf{n}}$ [1]. For a long time, attention has been drawn to a hypothetical biaxial nematic (N_b), on the ground of fundamental interest and the promise of faster switching times in display applications [2–4]. The N_b phase was theoretically described by Freiser [5] as being of orthorhombic symmetry with physical properties different along three mutually perpendicular directors $\hat{\mathbf{n}} \equiv -\hat{\mathbf{n}}$, $\hat{\mathbf{m}} \equiv -\hat{\mathbf{m}}$ and $\hat{\mathbf{l}} \equiv -\hat{\mathbf{l}}$. The existence of N_b was first shown in a lyotropic LC [6] but in thermotropic systems, N_b remained elusive, despite the intense search [7–13].

Address correspondence to O. D. Lavrentovich, Liquid Crystal Institute and Chemical Physics Interdisciplinary Program, Kent State University, Kent, OH 44242, USA. Tel.: +1 (330) 672-4844; Fax: +1 (330) 672-2796; E-mail: olavrent@kent.edu

The current focus of the search is on materials with molecules of unusual shape. First, Li et al. [14] demonstrated the N_b phase in the nematic material formed by cyclic (ring-like) molecules. The search expanded to the broad class of bent-core molecules after Niori et al. [15] had shown that they can form a biaxial smectic phase. As a result, a number of symmetric [16] and asymmetric [17] bent-core nematic compounds was synthesized and recently reported to exhibit N_b [17,18]. N_b was also detected in the liquid-crystalline polymers [19] and organo-siloxane tetrapodes [20], adding to the expansion of this field of LC research [21]. However, identification of the N_b phase in bent-core mesogens [4,17,18,22–25] is not universally accepted, and alternative, non-biaxial explanations of the observed features are offered [26–32].

The first bent-core materials for which the existence of the N_b phase has been reported on the basis of NMR [18c] and X-ray diffraction (XRD) [18a] studies were oxadiazole compounds ODBP-Ph-C_7 (C7) and ODBP-Ph-O-C_{12} (C12) [16]. The studies by Vaupotič et al. [29] on a different bent-core compound suggested that the XRD features attributed to N_b can be caused by pretransitional smectic C (SmC) order fluctuations (''cybotactic clusters'') that develop in N_u over an extended temperature range. Francescangeli and Samulski [31] performed an XRD study of a nematogen ODBP-Ph-O-C_4H_9, which belongs to the same series ODBP-Ph-O-C_nH_{2n+1} as C12. They concluded [31] that ''the cybotactic clusters of stratified and tilted mesogens embedded in an otherwise translationally disordered nematic host medium would engender motionally averaged second rank tensorial attributes that are biaxial, and this may account for the NMR biaxiality observed in nematic phases of ODBP mesogens'' [18c].

In the present work, we address the status of the uniaxial vs. biaxial nematic order in two bent-core oxadiazole materials C7 and C12, by exploring their stability at high temperatures, their optical and dielectric properties, as well as surface alignment and features of topological defects. We show that the experimentally observed features of C7 and C12 are consistent with the uniaxial N_u order.

2. Experiment

2.1. *Materials*

The two studied compounds, 4,4′(1,3,4-oxadiazole-2,5-diyl) di-*p*-heptylbenzoate (ODBP-Ph-C_7) and 4,4′(1,3,4-oxadiazole-2,5-diyl) di-*p*-dodecyloxybenzoate (ODBP-Ph-O-C_{12}) [16,18], were synthesized by Merck Corp. (Germany), Figure 1. We studied two types of samples: samples AR (as received from the manufacturer) and samples REC obtained by recrystallization of AR samples as described in Ref. [16]. In all our experiments, contact of REC samples with oxygen was minimized by using a special nitrogen-filled box (Fig. 2). The molecular structure and purity of AR and REC samples were verified by high-resolution ^{1}H and ^{13}C NMR spectroscopy, high performance liquid chromatography/mass spectroscopy (HPLC/MS) and elemental analysis (see Appendix), which showed no distinction in the composition of the two. However, the samples did show different behavior depending on whether they were exposed to the contact with oxygen and elevated temperatures, as described in details below.

The phase diagrams for C7 and C12 are the same for AR and REC samples (Fig. 1). The phase diagrams were obtained during cooling and are shown in

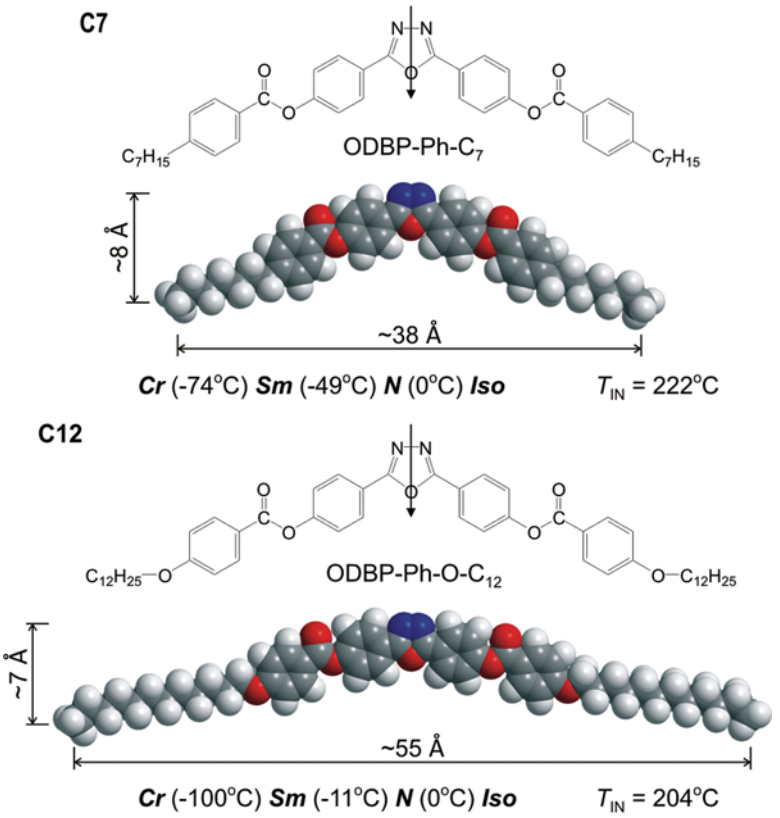

Figure 1. Molecular structure, model and phase sequence of thermotropic bent-core liquid crystals C7 and C12. The arrow shows the direction of the dipole moment. Molecular model shows space-filling structure. (Figure appears in color online.)

Figure 1 in terms of the reduced temperature $t = T - T_{IN}$, where T is the actual temperature and T_{IN} is the temperature of the isotropic (*Iso*) to nematic (*N*) phase transition. For C7, $T_{IN} = 222°C$ and for C12, $T_{IN} = 204°C$. One or more smectic phases with a tilted orientation of molecules within the smectic layers are denoted as *Sm*. XRD and NMR studies [18] suggested that N_b in C7 and C12 is stable over the entire temperature range of the nematic phase but subsequent electrooptic experiments [4,24b] suggested that N_b exists only at low temperature (below $t = -12°C$ for C7), so that the nematic range is split between the uniaxial and biaxial phases.

The experimental cells for optical and electrooptical studies were assembled from parallel glass plates with transparent indium tin oxide (ITO) electrodes. The tangential alignment was achieved by spin-coating polyimide films of PI2555 (HD MicroSystem), AL22620 and AL60702 (JSR Corp.) [24a] onto the ITO layers; the baking temperature was (220-275)°C. The tangential alignment of $\hat{\mathbf{n}}$ at unrubbed PI2555, AL22620 and AL60702 was established by observing half-integer disclinations in Schlieren textures [33]. For planar (unidirectional) alignment, the polyimide layers were rubbed 3–5 times with pressure (800–850) Pa and the cells were assembled in an "antiparallel" fashion. This resulted in a small pretilt angle (1–2)° between the substrate and the director $\hat{\mathbf{n}}$ measured by a crystal rotation method

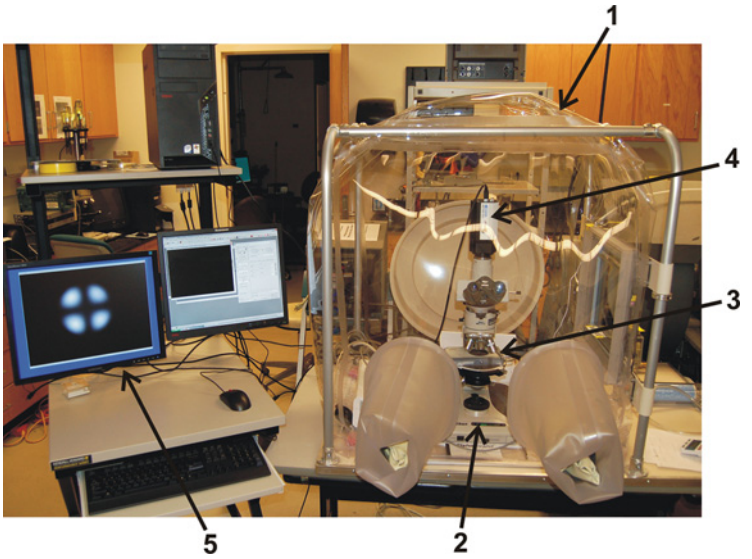

Figure 2. Experimental setup for studying optical properties and textures of C7 and C12 in the oxygen-free environment: 1 – vinyl glove box; 2 – polarizing microscope; 3 – hot stage with samples; 4 – CCD camera; 5 – computer with image acquisition software. (Figure appears in color online.)

[34]. To achieve a homeotropic alignment, we used an inorganic passivation layer NHC AT720-A (Nissan Chemical Industries, Ltd.) as well as freshly cleaned ITO-coated glass plates. Note that the terms "homeotropic" and "planar" alignment refer to the normal and unidirectional planar alignment of the main director $\hat{\mathbf{n}}$.

The cell thickness $d = (5–55)$ μm was set by glass spacers mixed with temperature cured epoxy paste EPO-TEK B9021 (Epoxy Technology) with a small coefficient of thermal expansion $6 \times 10^{-5}\,^{\circ}\mathrm{C}^{-1}$, which was used for sealing the cells. The actual thickness d was measured using the interference method [35]. The LC materials were filled into the cells in the isotropic phase, and all the experiments were performed by cooling from their *Iso* phase and keeping them within the *N* temperature range away from smectic phase.

2.2. *Experimental Methods*

The temperature was controlled with a Linkam controller TMS94 and a hot stage LTS120 (Linkam Scientific Instruments) with precision 0.01°C. An ac or dc voltage was applied to the cells using a function generator DS345 (Stanford Research System) and a wide band amplifier 7602 (Krohn-Hite). We used an impedance analyzer SI1260 (Schlumberger) for the dielectric spectroscopy measurements.

A polarizing microscope OptiPhot2-Pol (Nikon Instruments, Inc.) was used for orthoscopic observations. The image acquisition was realized with a CCD camera and image analyzing software ImagePro Plus 6.1 (Media Cybernetics, Inc.). Conoscopic studies under the microscope were performed with a Bertrand lens and high power objectives Nikon MPlan $20\times/\mathrm{NA} = 0.4$, $40\times/\mathrm{NA} = 0.5$, $60\times/\mathrm{NA} = 0.7$ ELWD (extra large working distance) with large numerical aperture (NA). A laser

conoscopic setup was built using the laser (Ion Laser Technology) with tunable wavelength ($\lambda = 514$ nm). To increase the quality of conoscopic observations, we also often used a "frosted" glass placed before the sample [36,37]. We used single wave (λ) and quarter wave ($\lambda/4$) plates with $\lambda = 530$ nm to determine the sign of birefringence and to characterize small variations of optical retardation [36,38]. A thick Berek compensator (Nikon Instruments, Inc.) was used to determine the direction of "slow axis" and measure birefringence. The spectral properties of C7 and C12 were studied with a microscope-mounted Photometry System P100S (Nikon Instruments, Inc.); the transmitted signal was measured from a circular area of diameter 40 μm. In the studies of topological defects, we used cylindrical glass capillaries of inner diameter 10 and 50 μm (VitroCom) and glass spheres of diameter 10 μm.

To study the samples REC of C7 and C12 in the oxygen-free environment, ~(10–100) ppm, we used the vinyl basic glove box (Coy Laboratory Products, Inc.) filled with dry nitrogen (Fig. 2). The experimental equipment and materials were loaded into the glove box prior to sealing and filling the nitrogen. The temperature (~30°C) and relative humidity (<10%) inside the glove box were measured with the conventional digital thermometer and hygrometer. The volume of oxygen was detected with the Quantek oxygen analyzer, model 200 (Quantek Instruments). The optical and conoscopic observations were performed via the CCD camera Micropublisher 5.0 RTV (QImaging).

High resolution NMR spectroscopy of studied materials was carried out in the Magnetic Resonance Center (The University of Akron, USA) using Varian Inova (750 MHz) for proton NMR and Varian NMRS (500 MHz) for carbon NMR experiments. The HPLC/MS analysis of the samples has been performed in the Chemistry Research Facilities of The University of Akron by using a liquid chromatograph Agilent 1100 (Agilent Technologies, Inc.) coupled with an Esquire ion trap mass spectrometer (Bruker Daltonics, Inc., Billerica). A C18 column was used for liquid chromatography separation and the mobile phase was THF-H_2O (tetrahydrofuran-water).

3. Results and Discussion

3.1. *Chemical Stability*

The bent-core materials C7 and C12 form the nematic phase at very high temperatures (Fig. 1) [16,18]. We explored the chemical stability of these compounds by keeping them at an elevated temperature 200°C for 2 hours. The AR samples were kept in the regular conditions (with an access of oxygen), while the REC samples were kept in the oxygen-free environment. The treatment did not cause any changes in the appearance of REC samples, but changed the color of AR samples from white to brownish, for both C7 and C12 compounds (Fig. 3).

Figure 4 demonstrates the effect of high temperature treatment on the NMR spectra of C7 samples. The NMR spectra of AR and REC samples before heating are the same (Fig. 4a). After heating in the oxygen-free environment, the spectrum of REC sample did not change (Fig. 4b). However, the spectrum of AR sample heated in the presence of oxygen (Fig. 4c) did change, revealing new peaks that indicate chemical degradation/decomposition.

The thermal gravimetric analysis (TGA) performed for the AR sample of C7 in the presence of oxygen shows significant weight loss with time when kept at high

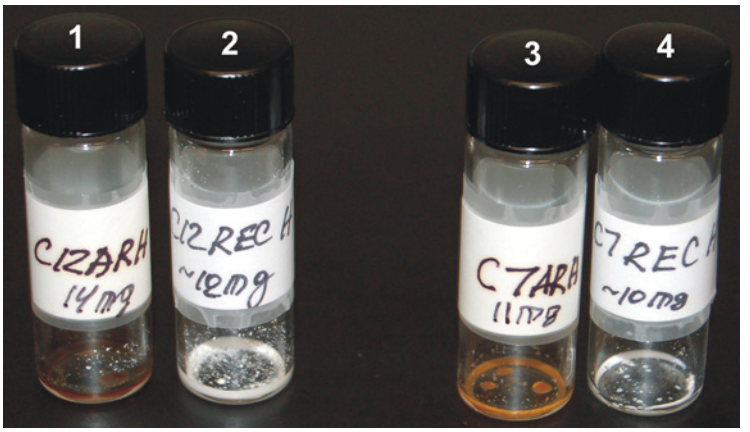

Figure 3. Samples of liquid crystals C12 (1, 2) and C7 (3, 4) after being kept in the nematic phase at 200°C for 120 min in the room (1, 3) and oxygen-free (2, 4) environment. Samples 1 and 3 show brown colors. (Figure appears in color online.)

temperature (Fig. 5). The weight loss increases when the temperature increases and is most significant in the *Iso* phase (Fig. 5). In contrast, TGA of C7 kept in the nitrogen atmosphere, did not show any significant weight losses even after the sample was kept at 195°C for ~20 hrs.

The experiments above show that C7 and C12 are chemically unstable and prone to degradation when kept at high temperatures in the presence of oxygen. Chemical degradation within the temporal scales of ~1 h can profoundly affect the properties of the materials (as we demonstrate below for the case of dielectric permittivity). Because of this, we performed our experiments not only in normal environment with

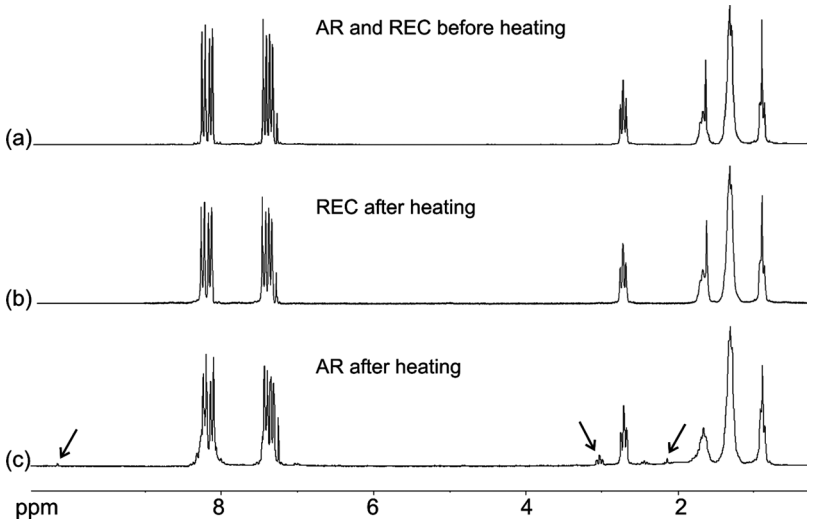

Figure 4. ^{1}H NMR (200 MHz) spectra of samples AR and REC of C7 before (a) and after (b,c) heating. Arrows show new peaks in the NMR spectrum of heated AR sample.

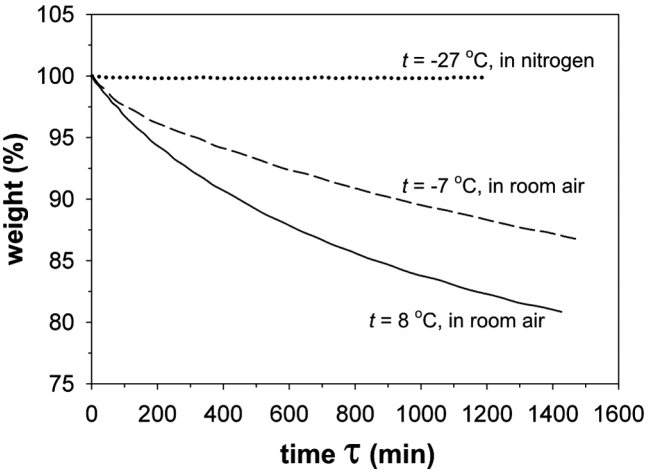

Figure 5. TGA for sample AR of C7 performed in the room and oxygen-free environment.

oxygen, but also in the nitrogen-filled glove box (Fig. 2) in which the contact with oxygen and degradation were minimized.

3.2. *Dielectric Properties*

We measured the dielectric dispersion of C7 and C12 (Fig. 6) and its temperature dependence. The dielectric measurements (Fig. 6a, b) in the nematic phase were made in the frequency range (0.1–1000) kHz on cooling the samples in the room environment. The measured real and imaginary dielectric permittivities ε' and ε'' have very large values at frequencies lower than 10 kHz, similar to ferroelectric LCs [39]. The ''cybotactic clusters'' with smectic C order [29,31,32] existing in the nematic phase of bent-core materials could be the reason for the large values of dielectric permittivity. The dielectric dispersion curves of C7 and C12 show Debye-like behavior [40] but the temperature dependencies are highly unusual. Namely, the relaxation time $\tau_c = (2\pi f_c)^{-1}$, where f_c is a relaxation frequency at which ε'' reaches its maximum, decreases when T decreases (Fig. 6a, b), which is opposite to the standard trend [41,42]. We attribute this unusual dependence to the chemical degradation at high T rather than to the temperature changes themselves. To confirm it, we measured the dielectric permittivities at $T = const$; the data revealed a strong dependence on time (Fig. 6c, d); ε' increased and τ_c decreased with time. Our interpretation is in agreement with NMR and TGA experiments (see Sec. 3.1) and with the notion that chemical degradation generates shorter fragments of main constituents and ionic impurities that reduce τ_c [43].

The dielectric constants $\varepsilon'_{\parallel}$ and $\varepsilon'_{\perp}$ (parallel and perpendicular to $\hat{\mathbf{n}}$) were measured in the cells with AT720-A and PI2555 alignment layers, respectively. To avoid chemical degradation of the materials, we measured the dielectric constants at 1 and 10 kHz in the *Iso* phase right after the filling materials into the cells and then in the N phase during the first 15 min of the experiment (Table 1). Both materials, C7 and C12, have a negative dielectric anisotropy $\Delta\varepsilon = \varepsilon'_{\parallel} - \varepsilon'_{\perp} < 0$ and, thus, the method for identification of the N_b phase based on conoscopic observations under the

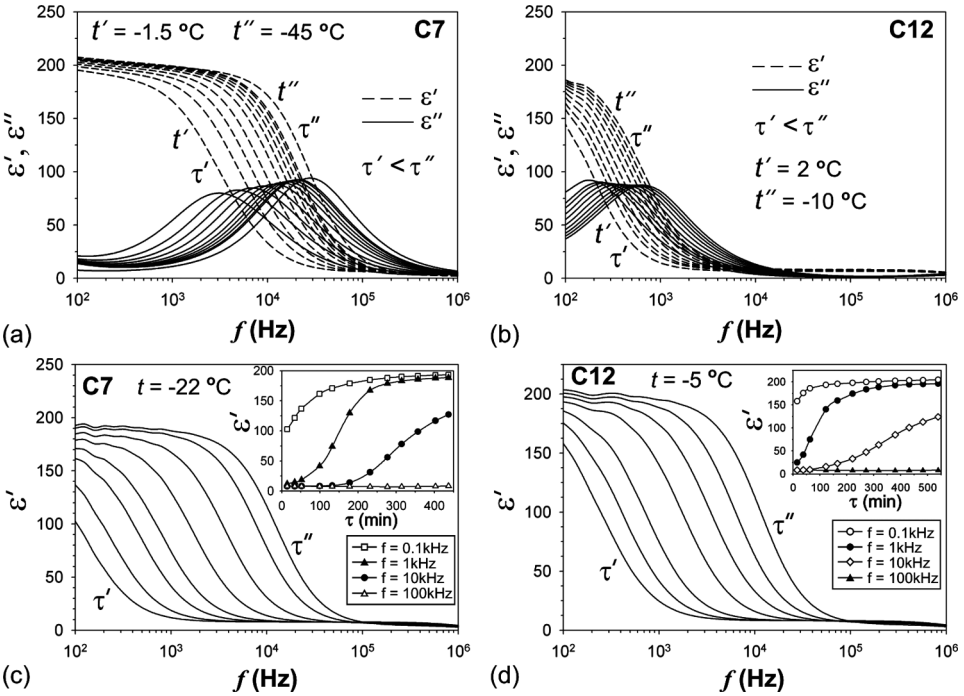

Figure 6. Dielectric properties of nematics C7 and C12 measured in the planar cell ($d = 11\,\mu m$) with PI2555 alignment layers: a, b) dielectric permittivities ε' and ε'' vs. frequency; c, d) dielectric permittivity ε' changes with time at constant temperature.

applied electric field, suitable for the materials with positive $\Delta\varepsilon$ [28], is not applicable in this case.

3.3. *Optical Properties and Surface Memory Effect in Planar Cells*

The orientation of the director $\hat{\mathbf{n}}$ in the planar cells with C7 and C12 was along the rubbing direction for the alignment agents PI2555, AL22620 and AL60702. We measured the temperature dependence of birefringence $\Delta n = n_{\parallel} - n_{\perp}$ of C7 and C12 (Fig. 7), using the linearly polarized light beam propagating normally through the cell (with the wavevector $\mathbf{k} \perp \hat{\mathbf{n}}$). The refractive indices $n_{\parallel}$ and $n_{\perp}$ are measured for light polarization $\hat{\mathbf{e}} \parallel \hat{\mathbf{n}}$ and $\hat{\mathbf{e}} \perp \hat{\mathbf{n}}$, respectively, and, in the N_u phase, are associated

Table 1. Dielectric permittivities measured for compounds C7 and C12

		C7		C12	
		$f = 1\,kHz$	$f = 10\,kHz$	$f = 1\,kHz$	$f = 10\,kHz$
$t = 5°C$	ε'_{iso}	10.2	6.3	7.7	6.9
	$\varepsilon'_{\parallel}$	7	5	6.5	4.9
$t = -2°C$	$\varepsilon'_{\perp}$	24.1	7.2	23	7.8
	$\Delta\varepsilon$	−17.1	−2.2	−16.5	−2.9

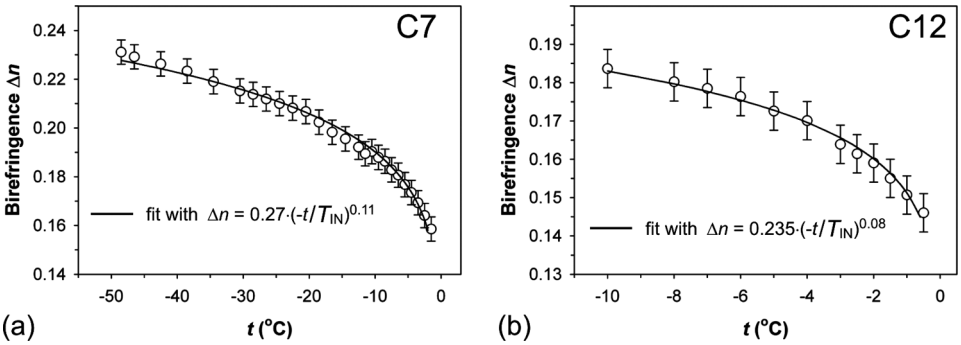

Figure 7. Birefringence Δn vs. temperature as measured with Berek compensator at 546 nm in the planar cells with C7 (a) and C12 (b). Error bar accounts for experimental error due to the cell thickness and measurement error of Berek compensator.

with the extraordinary n_e and ordinary n_o refractive indices, respectively. Using the Berek compensator, the birefringence Δn was determined as positive in the entire temperature range of the nematic phase. The temperature dependence follows an empiric law $\Delta n = A \cdot (-t/T_{IN})^{\beta}$ [44] with two adjustable parameters A and β and no abrupt changes (Fig. 7).

We observed a surface memory effect [45] in C12 planar cells with PI2555 alignment layers (Fig. 8). The unidirectionally aligned samples (Fig. 8a) were cooled down below the temperature t_{NS} to the *Sm* phase (Fig. 8b) and then reheated back into the *N* phase (Fig. 8c). The texture of reheated sample (Fig. 8c) preserves some features of the *Sm* texture (Fig. 8b), clearly visible when the polarizers are uncrossed (Fig. 8d, e). These smectic texture features persist even after heating the sample into the *Iso* phase and then cooling back into the *N* phase. Although the effect is of interest by itself, it

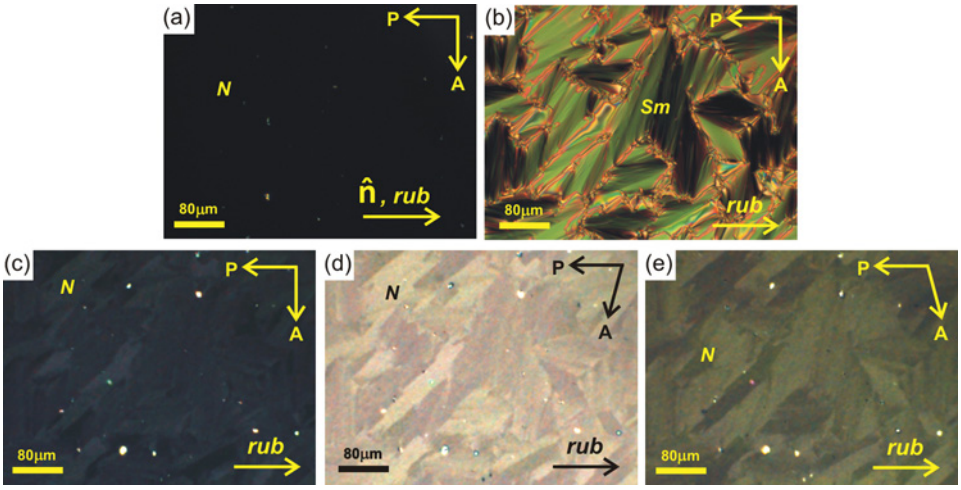

Figure 8. Surface memory effect in the planar cell with C12 and PI2555 alignment layers: a) planar alignment at $t = -5°C$; b) *Sm* focal conic texture at $t = -14°C$; c, d, e) nematic texture obtained upon heating from *Sm* phase, $t = -5°C$. (Figure appears in color online.)

interferes with the proper identification of the nematic ordering; because of this, we always kept the samples above the temperatures at which the materials form the *Sm* phase(s).

3.4. *Homeotropic Alignment and Its Temperature Dependence*

Homeotropic alignment in flat sandwich-type cells offers a straightforward approach to discriminate between N_u and N_b in optical observations. In the homeotropic N_u, the director $\hat{\mathbf{n}}$ is normal to the bounding plates. Orthoscopic transmission of linearly polarized light through such a cell does not depend on polarization $\hat{\mathbf{e}}$ and the refractive index $n_\perp$ measured in this geometry is the ordinary index n_o. However, in the homeotropic N_b state, the refractive index for the linearly polarized light should depend on the direction of $\hat{\mathbf{e}}$. The difference between the principal values of the refractive indices in such a biaxial cell, $\Delta n_{xy} = n_y - n_x$ is proportional to the degree of biaxial order. Therefore, one expects to observe a birefringent texture ($\Delta n_{xy} \neq 0$) if the order is biaxial and an extinct homeotropic state if the order is uniaxial.

In the experiment, we observe the classical homeotropic texture with $\Delta n_{xy} = 0$ in some temperature region $t_t \leq t \leq 0$ below the *Iso-N* phase transition, where t_t is in the range $-(22–38)$°C for C7 (AR samples) and $-(4–9)$°C for C12 (AR samples), changing from sample to sample. The REC samples studied in the oxygen-free environment showed a higher t_t, in the range $-(2–5)$°C for both C7 and C12.

Below t_t, the dark homeotropic textures (Fig. 9a, d) change to the textures of bright domains with random azimuthal orientations (Fig. 9b, e). One might attribute this transformation to the appearance of the N_b phase. Alternatively, the effect can

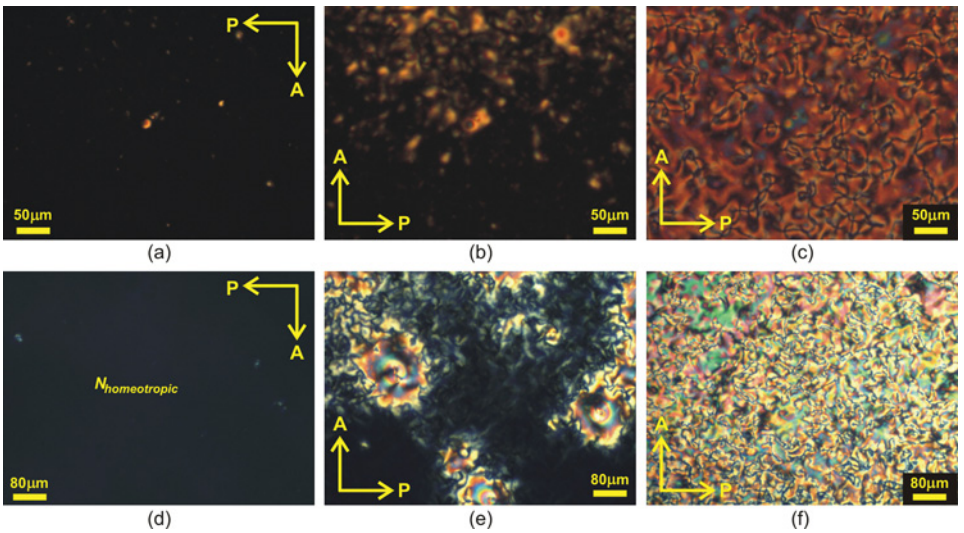

Figure 9. Anchoring transition in homeotropic cells between crossed polarizers. Top row shows REC sample of C7, $d \approx 9\,\mu m$: a) homeotropic orientation at $t = -3$°C; b) beginning of the anchoring transition at $t_t = -4$°C; c) tilted alignment at $t = -8$°C. Bottom row shows AR sample of C12, $d \approx 12\,\mu m$: d) homeotropic orientation at $t = -1$°C; e) beginning of the anchoring transition at $t_t = -4$°C; f) tilted alignment at $t = -6$°C. (Figure appears in color online.)

be caused by a surface anchoring transition (molecular tilt at the substrates). The retardation ($\Delta n_{xy}d$) increases as temperature decreases (Fig. 9b, c, e, f), reaching the values $\Delta n_{xy} \sim \Delta n$ characteristic for the tilted or even tangential orientation of the uniaxial phase. In temperature cycles, the bright domains nucleate repeatedly at the same irregularities (Fig. 9b, c, e, f); $\Delta n_{xy}d$ is not uniform over the cell area. Bright and dark domains coexist showing well defined boundaries (Fig. 9b, e). To explore the issue further, we used conoscopy [38].

3.5. *Conoscopic Observations of Homeotropic Samples*

Within the temperature range $t_t < t < t_{IN}$, both C7 and C12 show conoscopic images with isogyres that are slightly split by a small distance $2a$ (Fig. 10), even though the orthoscopic transmission of linearly polarized light through the cells did not depend on the direction of polarization $\hat{\mathbf{e}}$. Below t_t, the conoscopic images become fuzzy with no distinct features due to the small azimuthally degenerate domains (Fig. 9b, e).

One could estimate the possible biaxial optical anisotropy of the materials by assuming for a moment that the nonzero $2a$ is caused by biaxiality. In a uniformly aligned homeotropic N_b slab with three refractive indices $n_1 < n_2 < n_3$, the small value $2a$ is expressed through the so-called optic angle Φ: $\sin\Phi/2 = 2a \cdot \mathrm{NA}/(2R \cdot \bar{n})$ [46] and $\cos\Phi/2 = (n_1/n_2) \cdot [(n_3^2 - n_1^2)/(n_3^2 - n_2^2)]^{1/2}$ [38], where R is the radius of the field of view (Fig. 10d) and $\bar{n} = \sqrt{(n_e^2 + 2n_o^2)/3} \approx 1.6$ is the average refractive index [47]. Then from the expression $2a/2R = (\bar{n}/NA) \cdot (n_3/n_2) \cdot [(n_2^2 - n_1^2)/(n_3^2 - n_1^2)]^{1/2}$, one can estimate $\Delta n_{xy} = n_2 - n_1$. For the purpose of estimate, we associate the largest refractive index n_3 with the extraordinary index n_e measured in planar cells for $\hat{\mathbf{e}} \| \hat{\mathbf{n}}$

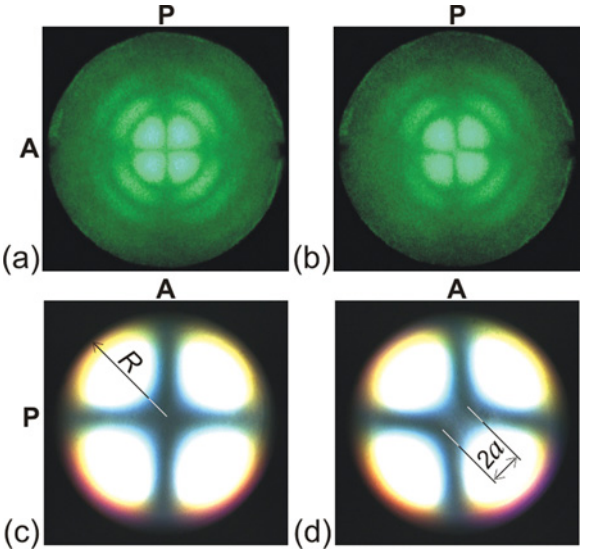

Figure 10. Conoscopic images for C7 material in the 52 μm thick homeotropic cell obtained with (a, b) laser conoscopic setup ($\lambda = 514$ nm) at $t = -5°$C and (c, d) taken under the microscope with objective Nikon MPlan $20\times$/NA = 0.4 at $t = -37°$C: (a, c) "cross" orientation; (b, d) sample is rotated 45° clockwise from "cross" orientation. P shows direction of polarizer, A shows direction of analyzer. (Figure appears in color online.)

and n_1 with the ordinary index n_o measured for $\hat{\mathbf{e}} \perp \hat{\mathbf{n}}$. We can use Δn measured in the C7 and C12 planar cells (Fig. 7) and determine n_e and n_o as $n_e \approx \bar{n} + 2\Delta n/3$ and $n_o \approx \bar{n} - \Delta n/3$. With $\Delta n \approx 0.22$ (Fig. 7a), $a/R = 0.138$ measured at $t = -37°C$ (Fig. 10d) and NA = 0.4 (Fig. 10c,d) we estimate $\Delta n_{xy} = 2 \times 10^{-4}$ for C7, indicating a very small degree of in-plane optical anisotropy as compared to $\Delta n = 0.22$. In a similar way, for C12 with $\Delta n \approx 0.18$ (Fig. 7b), $a/R = 0.18$ measured at $t = -7°C$ and NA = 0.4, we estimate $\Delta n_{xy} = 3 \times 10^{-4}$. In principle, nonzero values of $2a$ and Δn_{xy} estimated above for C7 and C12 might be considered as a feature of the (very weak) biaxial nematic order. An alternative explanation is that the two features are caused by a nonuniformity of the director tilt $\theta(z)$ along the normal (axis Z) to the bounding plates. In particular, the non-zero director tilt $\theta(z)$, in addition to causing the in-plane optical anisotropy, leads to a split of isogyres that can be estimated as $2a/2R = (\bar{n}/\mathrm{NA}) \cdot (\frac{1}{d}\int_0^d [\bar{\theta} - \theta(z)]^2 dz)^{1/2}$, where $\bar{\theta} = \frac{1}{d}\int_0^d \theta(z) dz$; $\theta(z)$ is the angle between the director and the axis Z. To distinguish between these two interpretations, one based on the idea of a homogeneous N_b and another one on the idea of inhomogeneous N_u, we study the conoscopic images in cells of different thickness d.

In a uniform "homeotropic" slab of N_b, the isogyres separation $2a$ represents the angle Φ between two optic axes that does not change with d [36,38,46]. Using the extended Jones matrix approach [48], we numerically simulated the intensity distribution in conoscopic images of hypothetical "homeotropic" (in the sense of the main director) biaxial samples of different thickness but with the same small $\Delta n_{xy} = 0.00264$ ($\Phi = 15°$) and verified that in the N_b cells, the separation $2a$ between the intensity minima is constant and independent of d (Fig. 11a–d).

We also simulated conoscopic images of N_u sample with a nonuniformly tilted $\hat{\mathbf{n}}(z)$, representing a thick homeotropic bulk region $\theta(z) = 0$ sandwiched between two subsurface layers with a non-zero $\theta(z)$ and birefringence (Fig. 11e–h). Two possible mechanisms can cause the formation of subsurface layers with a non-zero $\theta(z)$. First, the nematic phases in contact with a solid substrate are known to develop a density modulation along the normal to the cell, i.e., a layered smectic ordering which might propagate through several hundred nanometers [49]. In C7 and C12, this smectic ordering is expected to be of the tilted smectic C type, as the bulk smectic C phase appears below the nematic phase [16,18]. The second mechanism is related to the bent shape of C7 and C12 molecules and an ambiguity in the alignment of their two arms. In the N_u phase, vertical orientation of $\hat{\mathbf{n}}$ implies that each arm (Fig. 1) should make a non-zero angle $\phi/2 \approx 20°$ with the normal to the substrate, where $\phi \approx \pi - \psi$ and $\psi \approx 140°$ is the apex angle of the bent core of C7 and C12 [16,18]. However, if the surface sets a vertical alignment of one arm, then the second arm would have a tilt ϕ rather than $\phi/2$. The bulk of the sample and the subsurface layers might thus have a different tilt in the cell, stabilized by the smectic order near the substrates (and absence of such an order in the bulk). Figure 11e–g shows the conoscopic images calculated for such uniaxial ($\Delta n \approx 0.2$) cells with thick homeotropic bulk and two subsurface layers of thickness 500 nm each with the director tilted from the normal by 20°.

Our experimental conoscopic measurements (Fig. 12) show that the splitting $2a$ decreases when the cell thickness d increases, for both C7 and C12, studied in the room (Fig. 12d–f) and oxygen-free (Fig. 12a–c, g–i) environment. This behavior is consistent with the idea that the splitting is caused by the director field variation along the axis Z rather than by the bulk biaxiality. The surface-induced variation of the director is short ranged and in the cells with a macroscopic d in the range

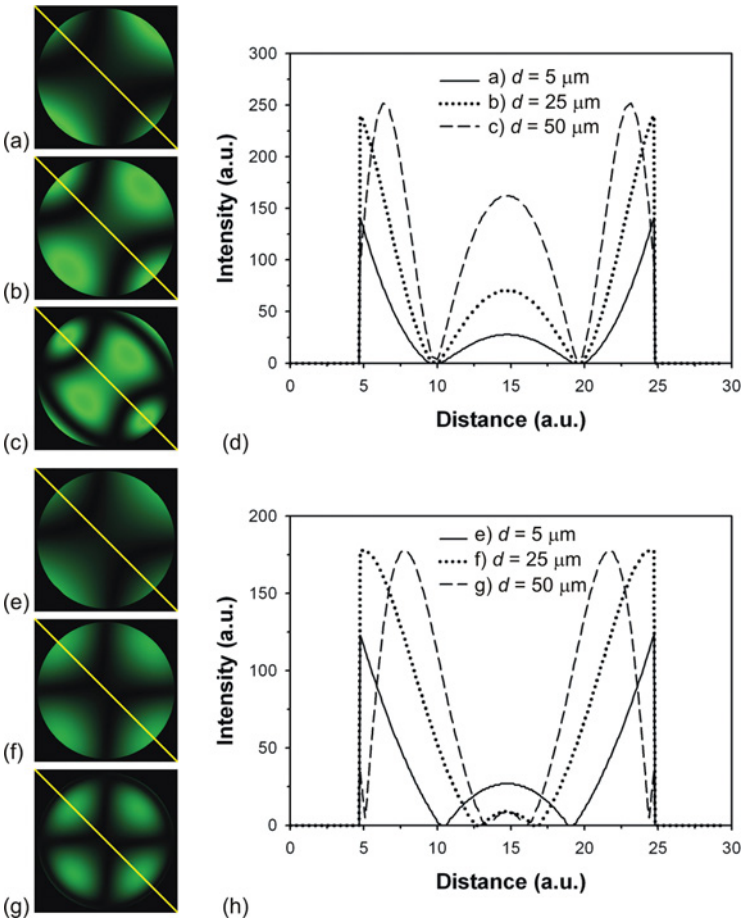

Figure 11. Calculated conoscopic images for the homeotropic biaxial (a,b,c) and vertically non-uniform homeotropic uniaxial (e,f,g) liquid crystal samples of different thickness d. Plots (d,h) show the transmitted intensity profile along the diagonal line in conoscopic images. Objective with NA = 0.4 and optic angle $\Phi = 15^\circ$ were used in calculations. (Figure appears in color online.)

of micrometers and tens of micrometers, the spatial scale of these distortions should be d-independent. When d increases, the main result is in the extension of the region in which the director remain parallel to the axis Z; as a result, the splitting distance $2a$ is expected to decrease in thicker cells, as observed.

3.6. *Topological Defects in Confined C7 and C12*

The N_u and N_b phases have different sets of topological defects, i.e., configurations of the order parameter ($\hat{\mathbf{n}}$ in N_u and $\hat{\mathbf{n}}$, $\hat{\mathbf{m}}$, $\hat{\mathbf{l}}$ in N_b) that cannot be continuously transformed into a uniform state [33,50]. Let us describe the distinctive features concerning the point (hedgehogs and boojums) and line (disclinations) defects.

In the bulk of N_u, topologically stable are point defects, such as a "hedgehog" with a radial $\hat{\mathbf{n}}(\vec{\mathbf{r}})$, and disclinations of strength $|s| = 1/2$; s is defined as a number

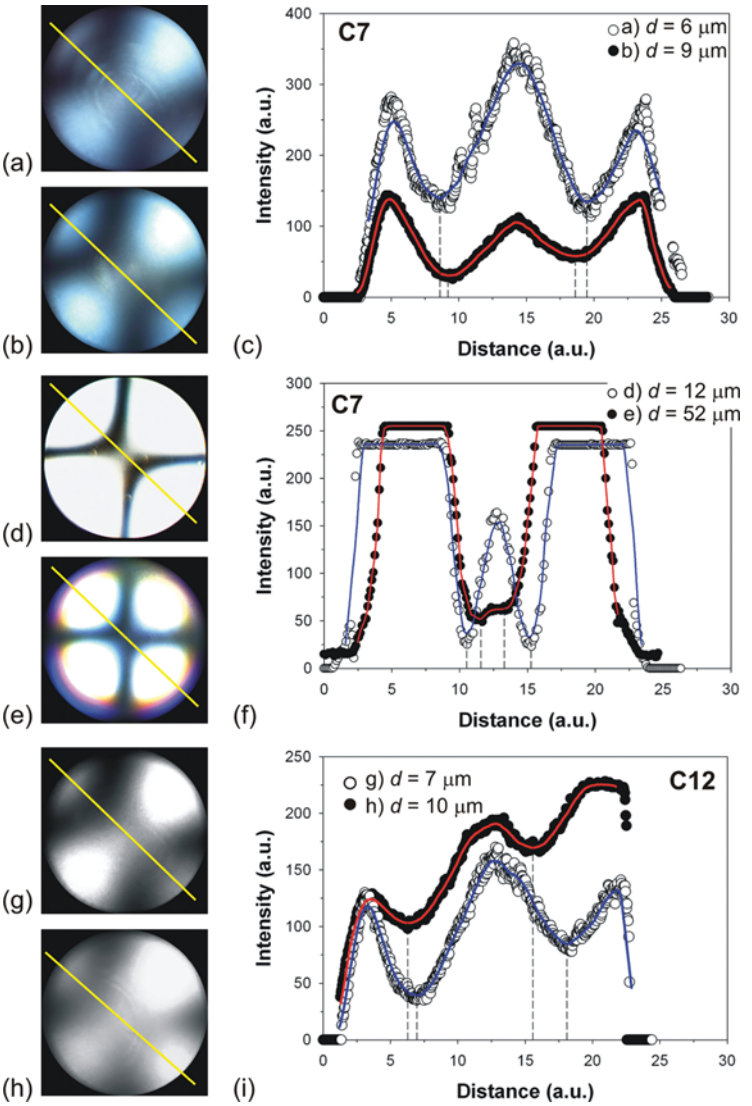

Figure 12. Experimental conoscopic images from the homeotropically aligned REC sample of C7 (a, b), AR sample of C7 (d, e) and REC sample of C12 (g, h) in the cells with different thickness; a, b, g, h) $t = -1°C$; d, e) $t = -35°C$. Plots (c, f, i) show the transmitted intensity profile along the diagonal line in conoscopic images. Objective with NA = 0.4 was used in the experiment. Open and filled circles show the measured data. Solid lines are eye guides to the experimental points and resulted from smoothing the data. (Figure appears in color online.)

of director turns by 2π when one circumnavigates the defect core once. Disclinations of strength $|s| = 1$ are not topologically stable. Even if the configuration with $|s| = 1$ is enforced by boundary conditions, for example, by confining N_u into a round capillary, $\hat{\mathbf{n}}$ would realign along the axis of the capillary [51a,52], a process called by Meyer an "escape into the third dimension" [52].

In the N_b phase, isolated point defects cannot exist: a radial configuration of one director implies that the two other directors are defined at a spherical surface and thus should form additional singularities emanating from the center of the defect, similarly to the "Dirac monopole" structure with a radial magnetic field and vector-potential perpendicular to it [33]. The disclinations can be of strength 1/2 and 1. In the case $|s| = 1$, the escape of one director does not remove the defect core, as two other directors restore the singularity.

At the surface of both N_u and N_b one can observe surface point defects - boojums. The strength s_b of a boojum at a surface of N_u with a tangential $\hat{\mathbf{n}}$ is defined by the number of director turns by 2π when one circumnavigates the defect core along the pathway at the surface; the smallest value is $s_b = 1$ as 1/2 would correspond to an end of a disclination [53]. In the N_b phase, the smallest value of s_b is 2; a defect with $s_b = 1$ represents an end of a singular disclination with $s = 1$.

3.6.1. *Escape of Director in a Round Capillary with C7 and C12.* We studied round capillaries with diameters 10 and 50 μm filled with C7 and C12 in their *Iso* phase and then slowly cooled (0.1°C/min) down into the *N* phase. To prevent the optical distortions caused by the round shape of glass capillary we placed them between two flat glass plates and filled the gap with an immersion oil of a refractive index 1.51 [51b]. The glass capillary provided homeotropic alignment and thus a radial director orientation near the walls, as established by polarizing microscopy. In the center of capillary, $\hat{\mathbf{n}}$ realigns along the axis, as expected for the N_u phase [51,52]. Since the two possible directions of the escape are of equal probability, cooling from the *Iso* phase results in a number of point defects-hedgehogs, of radial and hyperbolic type, separating the zone of different direction of escape (Fig. 13). The defects annihilate with each other, but this process slows down as the separation between the points become much larger than the diameter of the capillary, and thus interactions between them become weaker.

The textural features with the escaped non-singular core and isolated point defects do not change upon cooling the sample over the entire *N* temperature range; Figure 13a–c shows the typical textures for both materials at lower temperatures of the *N* phase. In the N_b phase one would expect the non-singular escaped configuration (Fig. 13a–d) either to transform into a single $s = 1$ defect line (Fig. 13e) with a singularity in the secondary directors [54], or to split into two lines with $s = 1/2$

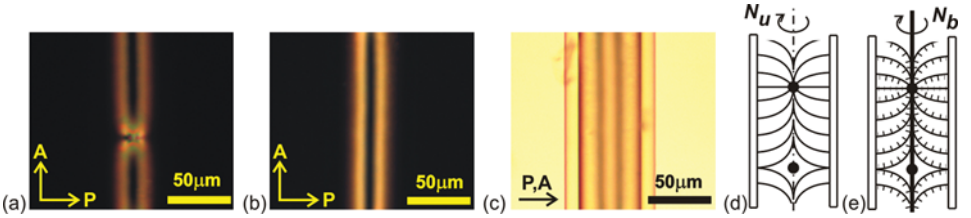

Figure 13. C12 at $t = -6$°C (a) and C7 at $t = -35$°C (b, c) in a round capillary (diameter 50 μm): a, b) crossed polarizers; c) parallel polarizers; (d) schematic of escaped director configuration in N_u showing point defects "hedgehogs" (black filled circles); (e) a hypothetical scheme of directors configuration in N_b with a nonsingular line defect of strength $s = 1$ with a singularity in the secondary directors (thick black line): solid lines show $\hat{\mathbf{n}}$ and short normal segments show one of the secondary directors. (Figure appears in color online.)

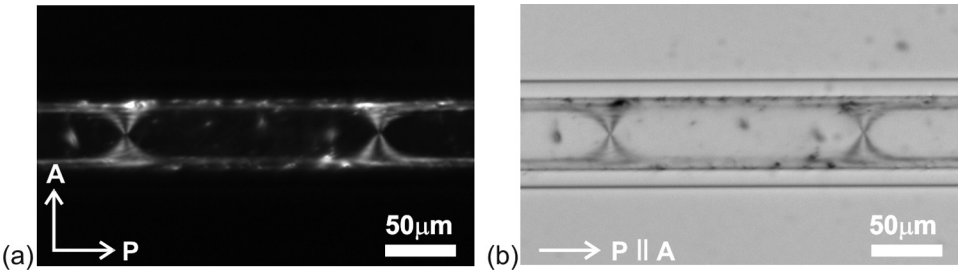

Figure 14. Sample REC of C7 in a round capillary in oxygen-free environment at $t = -42°C$: a) crossed polarizers; b) parallel polarizers.

each, as observed in the biaxial smectic A [55]. We observed neither of these N_b scenarios (Fig. 13a–c), despite our efforts to enhance the visibility of defects by using optical compensators. The textures in a capillary did not change their appearance below t_t. Thus the topological features of textures in cylindrical capillaries are consistent with the N_u order in the entire range of the nematic phase.

The REC samples of C7 and C12 filled in capillaries and studied in the oxygen-free environment showed similar uniaxial features of defects, with well-defined nonsingular disclinations and isolated point defects within the entire N temperature range (Figs. 14, 15). The REC sample of C7 showed no change of texture with isolated point defects (Fig. 14) above and below t_t. The textures of capillary filled with REC sample of C12 below $t_t = -3°C$ are distorted by the surface anchoring transition (Fig. 15b,c,e,f) rather than by transition into the biaxial phase, because the escape line preserved its internal structure and all changes occur near the surface. Comparing Figures 15b,c and 15e,f, one can see that distortions of the defects pattern reproduced themselves when the sample is heated above and cooled back below t_t, indicating the prime role of the surface interaction.

3.6.2. *Point Defects at Colloidal Spheres in C7 and C12.* We also explored the behavior of surface point defects-boojums and isolated point defects-hedgehogs formed at spherical inclusions immersed into the N phase [56,57]. Small spherical particles of

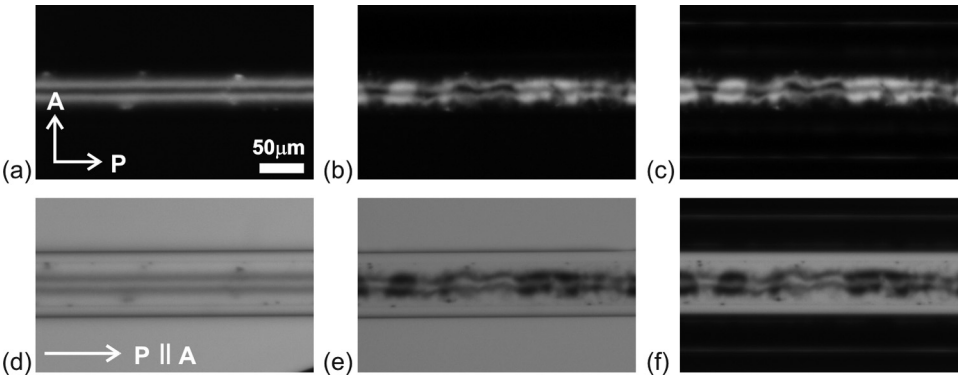

Figure 15. Sample REC of C12 in a round capillary in oxygen-free environment: a, d) $t = -2°C$; b, e) first cooling, $t = -6°C$; c, f) second cooling, $t = -6°C$.

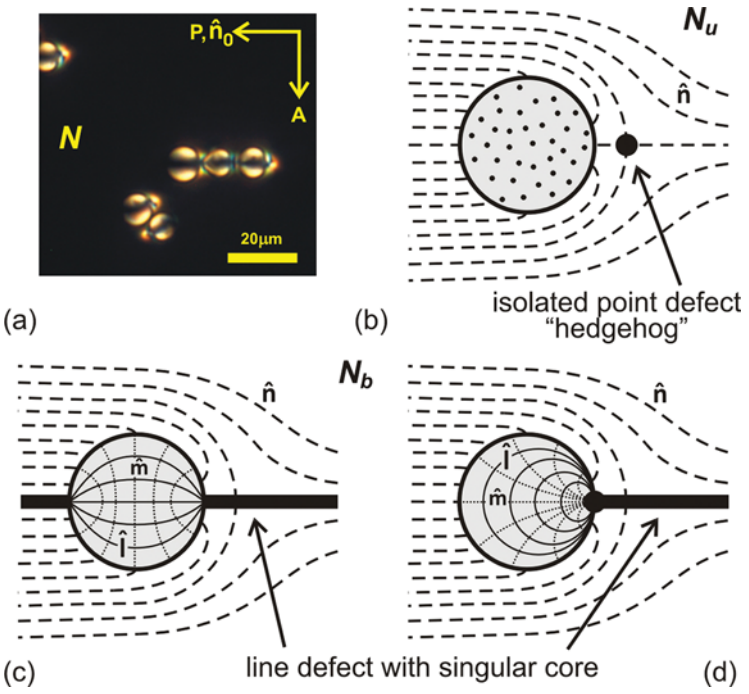

Figure 16. Colloidal solid glass spheres (diameter 10 μm) in a planar cell ($d = 25$ μm) with C12 at $t = -10°C$ (a); (b) scheme of director configuration around the particle in N_u; (c, d) a hypothetical schemes of director configuration around the particle in N_b. (Figure appears in color online.)

borosilicate glass (diameter 10 μm) and polystyrene (diameter 5 and 8 μm) were added to C7 and C12 and studied in planar cells of thickness $d = 25$ μm (Figs. 16, 17).

The glass spheres provided homeotropic alignment for C7 and C12 and the textures show a dipolar symmetry of distortions of $\hat{\mathbf{n}}$ with point defect, hedgehog, at one pole of the sphere (Fig. 16a, b), along the axis that is parallel to the direction of $\hat{\mathbf{n}}_0$ set by rubbing. This texture with hyperbolic hedgehog is valid for the N_u phase, but isolated point defects can not exist, as discussed above, in the N_b phase. Two solutions are possible, either a single line with singularity in minor directors emanating from the poles of the sphere parallel to the direction $\hat{\mathbf{n}}_0$ (Fig. 16c) or the surface boojum of $s_b = 2$ [33] with the emanating defect line with singularity in $\hat{\mathbf{m}}$ and $\hat{\mathbf{l}}$ (Fig. 16d). We did not observe any changes of dipolar textures (Fig. 16a, b) above and below t_t. Also, characteristic arrangements of spheres (Fig. 16a) remained unchanged in the entire N temperature range.

The samples with polystyrene spheres with tangential anchoring produced textures with a quadrupolar symmetry of distortions of $\hat{\mathbf{n}}$, with two point defects, boojums, at the poles of the sphere (Fig. 17a–c), along the axis that is parallel to $\hat{\mathbf{n}}_0$. Their existence is dictated by the topological requirement: a director field tangential to the surface of a sphere, should contain singularities with the total strength equal to the Euler characteristic of the sphere, which is 2: $\sum s_{b,i} = 2$ [33]. The texture with two isolated boojums at the poles is allowed in the N_u phase, but not in N_b. In the N_b phase, the relationship $\sum s_{b,i} = 2$ is still valid, but the isolated boojums of strength $s_b = 1$ cannot exist, as they should represent the ends of disclination lines of strength

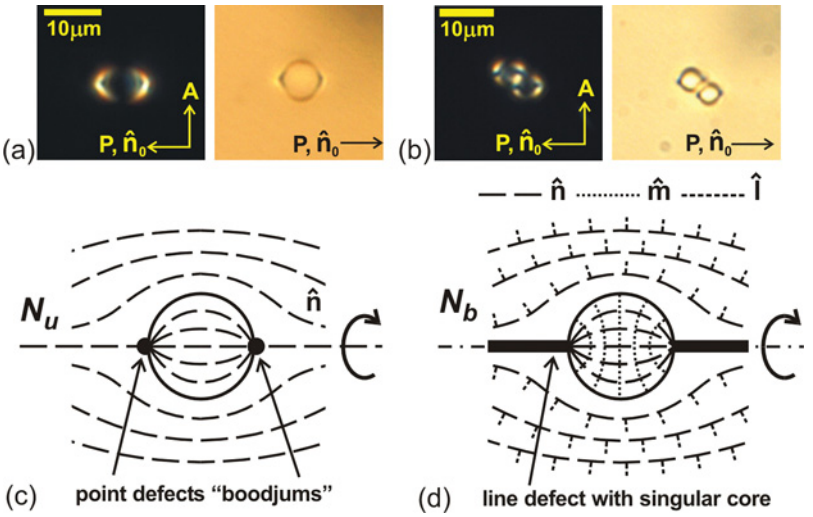

Figure 17. Colloidal solid polystyrene spheres in the planar cells ($d = 25\,\mu m$): a) C12, diameter $8\,\mu m$, $t = -6°C$; b) C7, diameter $5\,\mu m$, $t = -42°C$; (c) scheme of director configuration with "boojums" around the particle in N_u; (d) a hypothetical scheme of director configuration around the particle in N_b. (Figure appears in color online.)

$s = 1$ terminating at the surface of the spherical particle. The texture with boojums in our samples remained the same at all temperatures and did not extend into two singular lines $s = 1$ (Fig. 17a, b). There was also no tendency of the boojums to merge into a single boojum with $s_b = 2$ that is allowed in the N_b phase (Fig. 16d). Cooling down in the N temperature range did not perturb arrangements of particles with quadrupolar distortions (Fig. 17b). If there were disclinations terminating at the boojums, one would expect a rearrangement that would change the direction of particles' chains with respect to $\hat{\mathbf{n}}_0$ aimed at shortening the length of disclinations. Such rearrangements of colloids should be detectable even if the core of the disclinations are invisible under the microscope.

We facilitate the formation of equilibrium topologically non-trivial states even more by filling the capillary with glass spheres with homeotropic boundary

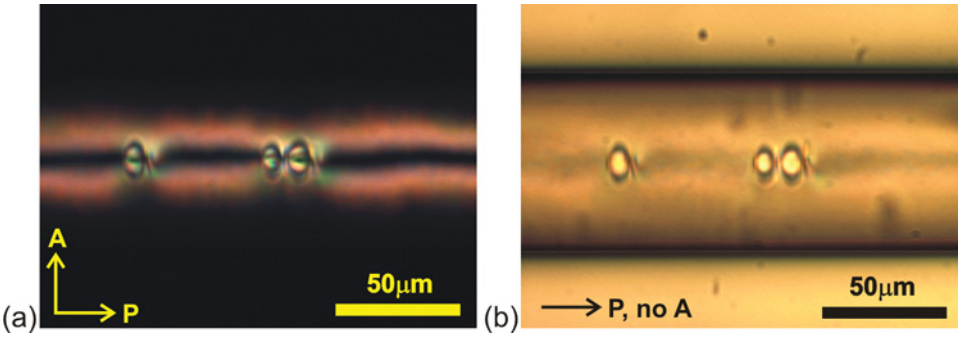

Figure 18. C12 in capillary at $t = -6°C$ with glass spheres (diameter was $5\,\mu m$): a) crossed polarizers; b) no analyzer. (Figure appears in color online.)

conditions (Fig. 18) as in Ref. [58]. In the N_b phase, such geometry is expected to show the texture with defect lines, singular in $\hat{\mathbf{m}}$ and $\hat{\mathbf{l}}$, connecting the spheres along the capillary axis. However, cooling down to t_{NS} did not result in any textural change and the N_u texture with escaped director and isolated point defects (Fig. 18) remained unchanged in both materials, C7 and C12.

Thus, the features of topological defects in samples with the three-dimensionally distorted $\hat{\mathbf{n}}$ considered above are fully consistent with the features of the uniaxial N_u phase but not with the expected properties of the N_b phase.

4. Conclusions

We studied dielectric dispersion, optical properties and topological defects of two thermotropic bent-core materials C7 and C12, to determine whether these materials have a biaxial nematic order. We found that the features of C7 and C12 are consistent with those of a uniaxial nematic N_u in the entire temperature range of the nematic ordering. The materials are unstable and prone to chemical degradation/decomposition at high temperatures (above 150°C) when studied for a long time (hours) in regular environment with oxygen.

We achieved a uniaxial homeotropic alignment of C7 and C12 using thin layers of AT720-A, in which case an orthoscopic light transmission does not depend on the direction of polarization in the plane of the cell, which is inconsistent with the presence of secondary directors of a biaxial phase. The homeotropic texture of C7 and C12 is stable within a certain range between the *N-Iso* phase transition and some temperature t_t that varies in a broad range depending on the substrate and presence of oxygen. Below t_t, the homeotropic texture changes to the texture of bright domains with random azimuthal orientations. Using conoscopy, we attribute this textural transformation to a surface anchoring transition rather than to the transition into the biaxial phase. The main feature of conoscopic textures is a small splitting of isogyres that decreases as the thickness of cell increases. The isogyres splitting is typically attributed to the biaxial order, but in our case, the splitting is associated with the non-uniform tilt of the uniaxial director along the normal to the plates. The nonuniformity along the normal to the bounding plates can be caused by surface-induced smectic layering and tilt of bent core molecules that is different from their orientation in the bulk.

We observed topological defects such as isolated point hedgehogs and boojums and nonsingular disclinations with an escaped director configurations that are characteristic of the N_u phase in the entire nematic temperature range and cannot be associated with the N_b phase.

After this manuscript has been accepted for publication, *Francescangeli et al.* published a paper [Francescangeli, O., Vita, F., Ferrero, C., Dingemans, T. & Samulski, E. T. (2011). *Soft Matter* 7, 895] presenting an X-ray diffraction (XRD) study on liquid crystals C7 and C12. The conclusion was that "the XRD data does not provide any direct support of the existence of a molecular biaxial nematic phase", similar to the conclusion achieved in our work.

Acknowledgment

The research was supported by Department of Energy, grant DOE-FG02-06ER 46331. We thank Samsung Electronics Corporation for the provided materials.

We thank V. M. Pergamenshchik, D. W. Allender, S. Kumar, Yu. A. Nastishin, and M. Mathews for discussions and suggestions.

We wish to thank the Kresge Foundation and donors to the Kresge Challenge Program at The University of Akron, The Ohio Board of Regents and The National Science Foundation (CHE-0341701 and DMR-0414599) for funds used to purchase the NMR instruments used in this work. We thank C. Wesdemiotis and V. Scionti for the help with HPLC/MS analysis.

Appendix

Chemical Compounds Characterization Data

C7, samples AR and REC: ^{1}H NMR (750 MHz, $CDCl_3$): $\delta = 8.21$ (d, 4H, Ar$\underline{H}$), 8.11 (d, 4H, Ar$\underline{H}$), 7.41 (d, 4H, Ar$\underline{H}$), 7.32 (d, 4H, Ar$\underline{H}$), 2.71 (t, 4H, α-C$\underline{H}_2$), 1.65-1.67 (m, 4H, β-C$\underline{H}_2$), 1.27-1.35 (m, 16H, $\gamma,\delta,\varepsilon,\zeta$-(C$\underline{H}$)$_2$-CH$_3$), 0.89 (t, 6H, ω-C$\underline{H}_3$) ppm; ^{13}C NMR ($CDCl_3$): $\delta = 162.94$ (C6), 162.33 (C1), 152.26 (C2), 148.4 (C10), 129.35 (C8), 127.82 (C9), 127.42 (C3), 125.57 (C7), 121.87 (C4), 120.65 (C5), 37.26, 33.01, 32.36, 30.51, 30.42, 24.09, 15.71 ppm; HPLC/MS (m/z): calcd. for $C_{42}H_{46}N_2O_5H$ [M + H], 659.34; found, 659.5; elemental analysis (Micro-Analysis, Inc.) for sample REC (calcd./found for $C_{42}H_{46}N_2O_5$): C (76.57/76.27), H (7.04/6.97), N (4.25/4.19), O (12.14/12.27).

C12, samples AR and REC: ^{1}H NMR (750 MHz, $CDCl_3$): $\delta = 8.2$ (d, 4H, Ar$\underline{H}$), 8.14 (d, 4H, Ar$\underline{H}$), 7.4 (d, 4H, Ar$\underline{H}$), 6.98 (d, 4H, Ar$\underline{H}$), 4.05 (t, 4H, α-C$\underline{H}_2$), 1.82-1.84 (m, 4H, β-C$\underline{H}_2$), 1.27-1.49 (m, 36H, $\gamma,\delta,\varepsilon,\zeta,\eta,\theta,\iota,\kappa,\lambda$-(C$\underline{H}$)$_2$-CH$_3$), 0.89 (t, 6H, ω-C$\underline{H}_3$) ppm; ^{13}C NMR ($CDCl_3$): $\delta = 162.64$ (C6), 162.36 (C1), 162.1 (C10), 152.34 (C2), 131.37 (C8), 127.4 (C3), 121.9 (C4), 120.57 (C5), 120.23 (C7), 113.82 (C9), 68.83, 31.16, 30.95, 30.93, 30.88, 30.85, 30.66, 30.4, 27.36, 24.14, 15.75 ppm; HPLC/MS (m/z): calcd. for $C_{52}H_{66}N_2O_7H$ [M + H], 831.49; found, 831.7.

References

[1] de Gennes, P. G., & Prost, J. (1993). *The Physics of Liquid Crystals*, Oxford University Press, Inc.: New York.
[2] Luckhurst, G. R. (2001). *Thin Solid Films*, *393*, 40.
[3] Berardi, R., Muccioli, L., & Zannoni, C. (2008). *J. Chem. Phys.*, *128*, 024905.
[4] Lee, J.-H., Lim, T.-K., Kim, W.-T., & Jin, J.-I. (2007). *J. Appl. Phys.*, *101*, 034105.
[5] Freiser, M. J. (1970). *Phys. Rev. Lett.*, *24*, 1041.
[6] Yu, L. J., & Saupe, A. (1980). *Phys. Rev. Lett.*, *45*, 1000.
[7] Malthête, J., Liébert, L., Levelut, A.-M., & Galerne, Y. (1986). *Acad, C. R., Sci., Ser. II: Mec., Phys., Chim., Sci. Terre Univers*, *303*, 1073.
[8] (a) Chandrasekhar, S., Sadashiva, B. K., Ratna, B. R., & Raja, V. N. (1988). *Pramana J. Phys.*, *30*, L491; (b) Chandrasekhar, S., Ratna, B. R., Sadashiva, B. K., & Raja, V. N. (1988). *Mol. Cryst. Liq. Cryst.*, *165*, 123.
[9] (a) Praefcke, K., Kohne, B., Gündogān, B., Demus, D., Diele, S., & Pezl, G. (1990). *Mol. Cryst. Liq. Cryst., Lett. Sect.*, *7*, 27; (b) Praefcke, K., Kohne, B., Singer, D., Demus, D., Pezl, G., & Diele, S. (1990). *Liq. Cryst.*, *7*, 589.
[10] Chandrasekhar, S., Nair, G. G., Praefcke, K., & Singer, D. (1996). *Mol. Cryst. Liq. Cryst.*, *288*, 7.
[11] (a) Chandrasekhar, S., Geetha, G. N., Shankar Rao, D. S., Prasad, S. K., Praefcke, K., & Blunk, D. (1998). Liq. Cryst., *24*, 67; (b) (1998). *Curr. Sci.*, *75*, 1042.

[12] Fan, S. M., Fletcher, I. D., Gündogān, B., Heaton, N. J., Kothe, G., & Praefcke, K. (1993). *Chem. Phys. Lett.*, *204*, 517.
[13] Hughes, J. R., Kothe, G., Luckhurst, G. R., Malthête, J., Neubert, M. E., Shenouda, I. G., Timimi, B. A., & Tittelbach, M. (1997). *J. Chem. Phys.*, *107*, 9252.
[14] Li, J.-F., Percec, V., Rosenblatt, Ch., & Lavrentovich, O. D. (1994). *Europhys. Lett.*, *25*, 199.
[15] Niori, T., Sekine, T., Watanabe, C., Furukawa, T., & Takezoe, H. (1996). *J. Mater. Chem.*, *6*, 1231.
[16] Dingemans, T. J., & Samulski, E. T. (2000). *Liq. Cryst.*, *27*, 131.
[17] Prasad, V., Kang, S.-W., Suresh, K. A., Joshi, L., Wang, Q., & Kumar, S. (2005). *J. Am. Chem. Soc.*, *127*, 17224.
[18] (a) Acharya, B. R., Primak, A., Dingemans, T. J., Samulski, E. T., & Kumar, S. (2003). *Pramana J. Phys.*, *61*, 231; (b) Acharya, B. R., Primak, A., & Kumar, S. (2004). *Phys. Rev. Lett.*, *92*, 145506; (c) Madsen, L. A., Dingemans, T. J., Nakata, M., & Samulski, E. (2004). *Phys. Rev. Lett.*, *92*, 145505; (d) Madsen, L. A., Dingemans, T. J., Nakata, M., & Samulski, E. (2006). *Phys. Rev. Lett.*, *96*, 219804.
[19] Severing, K., & Saalwäachter, K. (2004). *Phys. Rev. Lett.*, *92*, 125501.
[20] Merkel, K., Kocot, A., Vij, J. K., Korlacki, R., Mehl, G. H., & Meyer, T. (2004). *Phys. Rev. Lett.*, *93*, 237801.
[21] Luckhurst, G. R. (2004). *Nature (London)*, *430*, 413.
[22] Pelàez, J., & Wilson, M. R. (2006). *Phys. Rev. Lett.*, *97*, 267801.
[23] (a) Dong, R. Y., Kumar, S., Prasad, V., & Zhang, J. (2007). *Chem. Phys. Lett.*, *448*, 54; (b) Dong, R. Y., & Marini, A. (2009). *J. Phys. Chem. B*, *113*, 14062; (c) Yoon, H. G., Kang, Sh.-W., Dong, R. Y., Marini, A., Suresh, K. A., Srinivasarao, M., & Kumar, S. (2010). *Phys. Rev. E*, *81*, 051706; (d) Park, M. S., Yoon, B.-J., Park, J. O., Prasad, V., Kumar, S., & Srinivasarao, M. (2010). *Phys. Rev. Lett.*, *105*, 027801.
[24] (a) You, J., Jung, J. Y., Rhie, K., Pergamenshchik, V. M., & Shin, S. T. (2008). *J. Korean Phys. Soc.*, *52*, 342; (b) Lee, G.-S., Cho, J. S., Kim, J. C., Yoon, T.-H., & Shin, S. T. (2009). *J. Appl. Phys.*, *105*, 094509.
[25] Jang, Y., Panov, V., Kocot, A., Vij, J. K., Lehmann, A., & Tschierske, C. (2009). *Appl. Phys. Lett.*, *95*, 183304.
[26] Galerne, Y. (2006). *Phys. Rev. Lett.*, *96*, 219803.
[27] (a) Stannarius, R., Eremin, A., Tamba, M.-G., Pelzl, G., & Weissflog, W. (2007). *Phys. Rev. E*, *76*, 061704; (b) Stannarius, R. (2008). *J. Appl. Phys.*, *104*, 036104.
[28] Le, K. V., Mathews, M., Chambers, M., Harden, J., Li, Q., Takezoe, H., & Jákli, A. (2009). *Phys. Rev. E*, *79*, 030701(R).
[29] Vaupotič, N., Szydlowska, J., Salamonczyk, M., Kovarova, A., Svoboda, J., Osipov, M., Pociecha, D., & Gorecka, E. (2009). *Phys. Rev. E*, *80*, 030701(R).
[30] Tschierske, C., & Photinos, D. J. (2010). *J. Mater. Chem.*, *20*, 4263.
[31] Francescangeli, O., & Samulski, E. T. (2010). *Soft Matter*, *6*, 2413.
[32] Hong, S. H., Verduzco, R., Williams, J. C., Twieg, R. J., DiMasi, E., Pindak, R., Jákli, A., J. Gleeson, T., & Sprunt, S. (2010). *Soft Matter*, *6*, 4819.
[33] Kleman, M., & Lavrentovich, O. D. (2003). *Soft Matter Physics: An Introduction*, Springer-Verlag, Inc.: New York.
[34] (a) Scheffer, T. J., & Nehring, J. (1977). *J. Appl. Phys.*, *48*, 1783; (b) Le, K. V., Dhara, S., Sadashiva, B. K., Takanishi, Y., & Takezoe, H. (2006). *Jpn. J. Appl. Phys.*, *45*, L1013.
[35] Born, M., & Wolf, E. (1999). *Principles of Optics*, Cambridge Unversity Press: Cambridge.
[36] Hartshorne, N. H., & Stuart, A. (1970). *Crystals and the Polarising Microscope*, Edward Arnold (Publishers) Ltd.: London.
[37] Nastishin, Yu. A., & Pishnyak, O. (2009). *Personal Communication*.
[38] Wahlstrom, E. E. (1969). *Optical Crystallography*, John Wiley & Sons, Inc.: New York.

[39] Biradar, A. M., Kilian, D., Wrobel, S., & Haase, W. (2000). *Liq. Cryst.*, *27*, 225.
[40] (a) Yin, Y., Shiyanovskii, S. V., Golovin, A. B., & Lavrentovich, O. D. (2005). *Phys. Rev. Lett.*, *95*, 087801; (b) Gu, M., Yin, Y., Shiyanovskii, S. V., & Lavrentovich, O. D. (2007). *Phys. Rev. E*, *76*, 061702.
[41] Druon, C., Wacrenier, J. M., Hardouin, F., Tinh, N. H., & Gasparoux, H. (1983). *J. Phys. France*, *44*, 1195.
[42] Salamon, P., Éber, N., Buka, Á., Gleeson, J. T., Sprunt, S., & Jákli, A. (2010). *Phys. Rev. E*, *81*, 031711.
[43] Jin, M. Y., & Kim, J. J. (2001). *J. Phys.: Condens. Matter*, *13*, 4435.
[44] Le, K. V., Dhara, S., Sadashiva, B. K., Takanishi, Y., & Takezoe, H. (2006). *Jpn. J. Appl. Phys.*, *45*, L1013.
[45] Clark, N. A. (1985). *Phys. Rev. Lett.*, *55*, 292.
[46] Rittmann, A. (1963). *Swiss Bull. Mineral. Petrol.*, *43*, 11.
[47] Olivares, J. A., Stojadinovic, S., Dingemans, T., Sprunt, S., & Jákli, A. (2003). *Phys. Rev. E*, *68*, 041704.
[48] (a) Lien, A. (1990). *Appl. Phys. Lett.*, *57*, 2767; (b) Lien, A. (1997). *Liq. Cryst.*, *22*, 171; (c) Chen, C.-J., Lien, A., & Nathan, M. I. (1997). *J. Opt. Soc. Am. A*, *14*, 3125.
[49] Ruths, M., Steinberg, S., & Israelachvili, J. N. (1996). *Langmuir*, *12*, 6637.
[50] Toulouse, G. (1977). *J. Phys. (France) Lett.*, *38*, L67.
[51] (a) Cladis, P. E., & Kleman, M. (1972). *J. Phys. France*, *33*, 591; (b) Williams, C. E., Cladis, P. E., & Kleman, M. (1973). *Mol. Cryst. Liq. Cryst.*, *21*, 355.
[52] Meyer, R. B. (1973). *Philos. Mag.*, *27*, 405.
[53] Volovik, G. E., & Lavrentovich, O. D. (1983). *Zh. Eksp. Teor. Fiz.*, *85*, 1997; (1983). *Sov. Phys. JETP*, *58*, 1159.
[54] Chiccoli, C., Feruli, I., Lavrentovich, O. D., Pasini, P., Shiyanovskii, S. V., & Zannoni, C. (2002). *Phys. Rev. E*, *66*, 030701(R).
[55] Smalyukh, I. I., Pratibha, R., Madhusudana, N. V., & Lavrentovich, O. D. (2005). *Eur. Phys. J. E*, *16*, 179.
[56] Kleman, M., & Lavrentovich, O. D. (2006). *Philos. Mag.*, *86*, 4117.
[57] Poulin, P., & Weitz, D. A. (1998). *Phys. Rev. E*, *57*, 626.
[58] Kossyrev, P., Ravnik, M., & Žumer, S. (2006). *Phys. Rev. E*, *96*, 048301.